THE JOURNAL OF PHYSICAL CHEMISTRY A

 VOLUME 104, NUMBER 47, NOVEMBER 30, 2000

LETTERS

Reversible Oxidation Effect in Raman Scattering from Metallic Single-Wall Carbon Nanotubes

Zhonghua Yu and Louis E. Brus*

Department of Chemistry, Columbia University, New York, New York 10027

Received: June 16, 2000; In Final Form: August 23, 2000

Raman scattering from individual single-wall carbon nanotube (SWNT) bundles was measured using confocal optical microscopy with 632 nm laser excitation. The Raman scattering from metallic SWNTs was found to depend sensitively on adsorbed oxidizing molecules. Tangential mode Raman lines of HNO_3-treated SWNTs exhibited different line shapes from those of H_2SO_4/H_2O_2-treated SWNTs. However, the line shapes became identical after high power laser irradiation, which heats the bundle to ~750 K based on measurement of the breathing mode Stokes to anti-Stokes Raman intensity ratio. Thermal annealing of both samples at 873 K caused the same change in Raman spectra as with laser irradiation, which is attributed to degassing of doping adsorbates. A mechanism of charge transfer between carbon nanotubes and adsorbate molecules is proposed to explain the large change in Raman scattering from metallic SWNTs upon chemical doping and degassing. Raman scattering from degassed SWNT bundles was found to show a linear dependence on excitation intensity, suggesting that Raman cross sections do not change with temperature in the range 300−750 K.

Introduction

Since their discovery in 1993,[1,2] single-wall carbon nanotubes (SWNTs) have been a research field of great interest due to their potential applications in nanoscale devices.[3] An ideal SWNT can be viewed as a graphene sheet rolled up into a seamless cylindrical tube. SWNTs are predicted to be semiconducting or metallic depending on chirality.[3,4] Extensive experimental and theoretical efforts are being pursued to explore their electronic, vibrational, and mechanical properties.[3,5]

Raman scattering is a valuable tool to characterize SWNTs.[6−8] There are two phonon modes that give strong Raman scattering: the radial breathing mode (RBM) near 190 cm^{-1} and the tangential C−C stretching mode at about 1580 cm^{-1}. The radial breathing mode frequency is predicted to depend sensitively on the diameter of the tubes.[9] So Raman scattering can be used to estimate the size distribution of a SWNT sample. More interestingly, in Raman scattering from metallic carbon nanotubes, the tangential C−C stretching mode near 1580 cm^{-1} was observed to show a complex broadened line shape.[6,10] However, the origin of this line shape is still unclear; it has been fit by either a set of Lorentzians[10] or a Breit−Wigner−Fano (BWF) line shape function.[11]

Previous Raman scattering measurements of SWNTs were carried out with ensemble samples; the Raman spectra were averaged over the size, orientation, and the chirality of tubes. To get more insight into the vibrational properties, it is essential to be able to measure Raman scattering from individual bundles and even single tubes. Recently, surface-enhanced Raman scattering (SERS) has been applied to individual bundles of SWNTs (perhaps single tubes),[12,13] but modification of the resulting spectra due to the SERS effect is not well understood. We have been able to measure Raman scattering from individual bundles without SERS. In this letter we report that the characteristic broadened metallic Raman line can be fit very well by a Fano line shape function, and it depends sensitively on the processing conditions. This dependence appears to

10.1021/jp002197n CCC: $19.00
Published on Web 11/05/2000

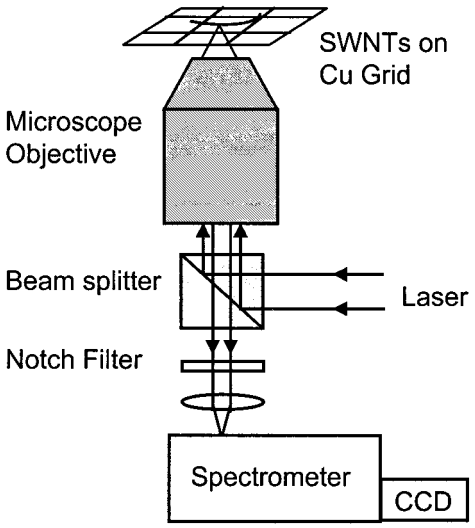

Figure 1. Schematic diagram of confocal Raman microscopy with a TEM grid as the substrate.

represent charge transfer between carbon nanotubes and adsorbed oxidizing molecules. Analogous effects have been recently observed in SWNT conductance experiments.[14,15] The temperature dependence of the Raman scattering is also reported as oxidation and temperature-induced degassing are closely related.

Experimental Section

SWNT material (diameter distribution ~1.05−1.5 nm, peaked at 1.2 nm) was bought from Tubes@Rice (Houston, TX). This material was synthesized by laser ablation, purified by refluxing in nitric acid, and redispersed in Triton x-100 aqueous solution of pH 10.[16] The original suspension of HNO_3-treated SWNTs was filtered through a polycarbonate membrane filter (3.0 μ pore size) and washed with methanol to remove the surfactant. The "bucky paper" formed on the membrane filter was peeled off and soaked in dimethyl formamide (DMF) for about three weeks. Then it was sonicated in DMF for about 1 h to obtain a stable homogeneous suspension of bundles and tubes. Alternatively, SWNTs were precipitated from the original suspension by addition of methanol and subsequent centrifugation. They were then sonicated in a mixture of H_2SO_4 and H_2O_2 (96% H_2SO_4:30% H_2O_2 = 4:1) for 30 min. After being filtered with a polyester membrane filter, they were redispersed in DMF with the aid of slight sonication. AFM examination shows that single bundles typically are about 10 nm in diameter and thus contain roughly 100 SWNTs.

The experimental setup is schematically shown in Figure 1. A 1000 mesh bare Cu TEM grid was used as the substrate. The SWNT suspension in DMF was spin cast onto the Cu grid. Raman measurements were taken with a Nikon TE300 inverted optical microscope in the epi-fluorescence mode. A cube beam splitter was used instead of a dichroic mirror in order to measure anti-Stokes Raman scattering. Dark field optical microscopy was used to first find the single bundles crossing over the 19 μm holes of the Cu grid. 632.8 nm HeNe laser light (4.5 mW) was focused by a microscope air objective (NA 0.8, 125×) onto one ~0.5 μm spot on the SWNT bundle. Raman scattering was collected by the same objective and focused onto the entrance slit of a single-stage spectrometer with a resolution of 4 cm^{-1}. A liquid nitrogen-cooled CCD camera recorded the spectra. A holographic notch filter (Kaiser Optical) was mounted in front of the spectrometer to reject the Rayleigh scattering light.

Results and Discussion

A. Raman Scattering from Metallic SWNTs. We have been able to successfully measure Raman scattering from individual bundles with exciting laser intensities as low as 3 kw/cm^2, because in our setup substrate scattering is eliminated and thus the signal-to-noise ratio is high. Figure 2 displays the Raman spectra in the 1270−1670 cm^{-1} region from individual SWNT bundles with 632 nm excitation. We found that the tangential mode Raman scattering depended sensitively on the processing conditions. After the bundle was excited by high power 632 nm laser light, the tangential mode Raman spectra of SWNTs underwent an irreversible change. Figure 2a shows the Raman spectra taken on one spot on one HNO_3-treated SWNT bundle. First at 3.3 kw/cm^2, there are two peaks: one at ~1560 cm^{-1} and one at 1590 cm^{-1}. At an excitation intensity of 340 kw/cm^2, a new, broad 1540 cm^{-1} peak is superimposed. When the power was lowered to 3.3 kw/cm^2 again, this new broad peak remains present. We observed this irreversible change in every bundle studied. Figure 2b shows the tangential mode Raman spectra from a H_2SO_4/H_2O_2-treated SWNT bundle. We notice that the tangential mode Raman line shape with low power excitation is distinctively different from that of the HNO_3-treated SWNTs. In H_2SO_4/H_2O_2-treated sample, the Raman component at 1560 cm^{-1} is suppressed and the line shape is narrowed. However, after high power laser irradiation, the Raman spectrum exhibits a large irreversible change similar to Figure 2a. In both cases, if we examine a different spot on the bundle, the original low power spectrum is observed.

Laser irradiation will heat the sample; Rinzler et al. previously used laser irradiation to heat multiwall carbon nanotubes.[17] In our case, the local temperature of the spot on a bundle under high power 220 kw/cm^2 laser irradiation is estimated to be ~750 K on the basis of the RBM Stokes to anti-Stokes Raman intensity ratio (see B below). To test whether this large irreversible change in Raman scattering is due to sample heating and therefore degassing, we put the Cu grid with SWNTs in a furnace and heated the SWNTs at 400 °C in flowing argon for 2 h. Then Raman scattering was measured again with low excitation power. Thermal treatment had the same effect on Raman scattering as high power laser irradiation, as shown in Figure 2c. After heating the sample, we obtained the same Raman spectra for both samples. Also the spectra are same as or similar to the Raman spectra after laser irradiation of the samples.

Raman scattering from SWNT bundles has been shown experimentally[6] and theoretically[18] to be a resonant process, associated with intense optical transitions between mirror-image spikes in the electronic density of states (DOS). The 632 nm Raman scattering of bulk material is dominated by contribution from metallic carbon nanotubes, and shows a characteristic broadened 1540 cm^{-1} mode line shape.[6,10] In prior ensemble studies, this broadening in metallic carbon nanotubes is absent in semiconducting tubes, which are resonantly excited at 457 nm. In our experiment, we find essentially this same result with a degassed single bundle. With 457 nm excitation the sharp Raman lines from semiconducting SWNTs did not exhibit a similar irreversible change as in metallic SWNTs. Also, we did not observe any irreversible change in the breathing mode Raman scattering for 632 nm excitation. The weak disorder Raman peak at ≈1325 cm^{-1} is unchanged upon heating, thus indicating that the observed effect is not due to annealing of structural defects.

The broadened 1540 cm^{-1} Raman line in metallic SWNTs has been tentatively interpreted as resulting from coupling of

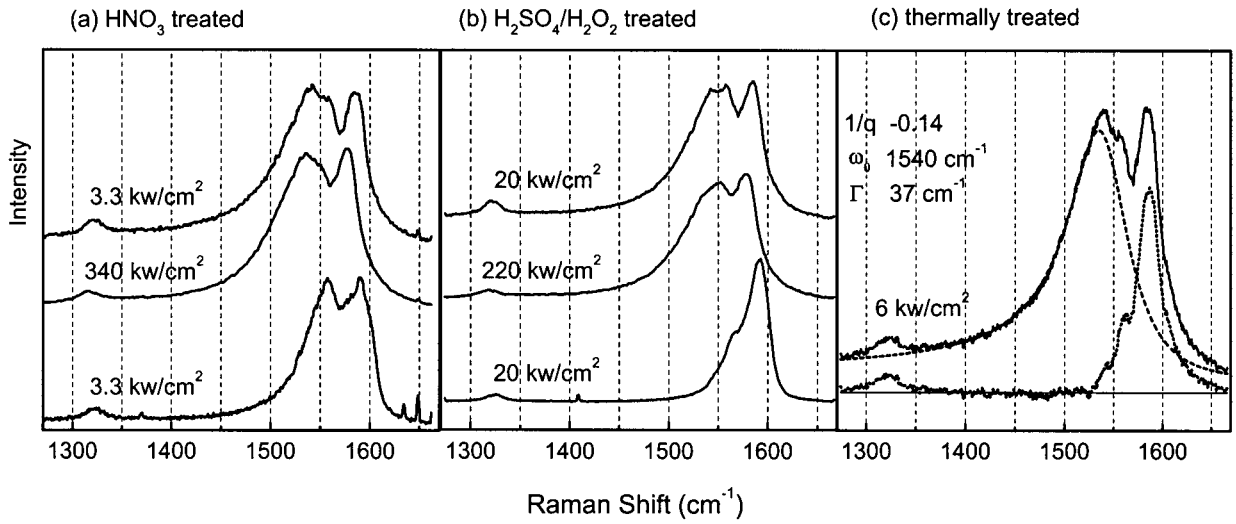

Figure 2. Laser irradiation effect on the tangential mode Raman spectra of (a) HNO_3-treated and (b) H_2SO_4/H_2O_2-treated SWNT bundles. The excitation wavelength was 632 nm. From bottom to top the spectra were measured consecutively from the same spot on the bundle. (c) Typical Raman spectrum of thermally treated SWNT bundles. The dashed curve is a BWF line shape function fit to the 1540 cm^{-1} Raman line, with the parameters indicated in the figure. The dotted curve is the remaining spectrum after subtracting the BWF fit from the typical Raman spectrum (solid curve).

phonon with isoenergetic electronic states.[11] Following Kataura et al.,[11] the broadened peak from a degassed single bundle is well fit with a Breit−Wigner−Fano (BWF) line shape function:

$$I(\omega) = I_o\{1 + (\omega - \omega_o)/q\Gamma\}^2/\{1 + [(\omega - \omega_o)/\Gamma]^2\}$$

where I_o, ω_o, Γ, and q, indicated in Figure 2c, are intensity, renormalized frequency, broadening parameter, and the line shape parameter, respectively. After subtracting the BWF line shape function, the remaining spectrum suggestively looks like the Raman spectrum of H_2SO_4/H_2O_2-treated bundles with low power 632 nm excitation. Nevertheless the clear identification of these Raman lines needs further study.

The observed large change in Raman scattering from metallic carbon nanotubes upon doping and degassing can be rationalized by considering the interaction with adsorbed oxidizing species. The electrical conductance of SWNTs is very sensitive to exposure to gases such as NO_2 and NH_3;[14] the large reversible change in conductance observed was interpreted to result from charge transfer doping. We propose that a similar charge transfer between SWNTs and oxidizing doping molecules is responsible for our observed effects. Charge transfer between the carbon nanotube and the copper grid should be negligible because they have similar work functions. Apparently the lowered Fermi level causes the weaker 1540 cm^{-1} metallic Raman line in HNO_3-treated sample and the strong suppression of 1540 cm^{-1} Raman component in H_2SO_4/H_2O_2 treated sample. One might suggest two possible mechanisms for the effect of charge transfer on Raman scattering from metallic carbon nanotubes. One involves the change in resonant electronic absorption properties of SWNTs upon chemical doping, which has been reported by some groups.[19,20] However, we observed that H_2SO_4/H_2O_2 oxidation produced no apparent change in the visible metallic electronic transition at low resolution, as observed in extinction spectra of SWNT suspensions. This implies that the oxidized Fermi level lies above the $n = 1$ state in the valence band. Rather, oxidative doping seems to affect the phonon structure and coupling to isoenergetic electronic states above the shifted Fermi level. A Fano line shape that depends sensitively on doping level has been observed in n-type degeneratively doped Si.[21] Also the 632 nm breathing mode Raman scattering is independent of oxidation, consistent with theoretical predictions[22,23] that long-range deformations do not couple to propagating electronic states in metallic tubes.

In agreement with previous work,[10,11] we assign the broadened 1540 cm^{-1} Fano Raman peak to the metallic tubes in the bundle. We suspect, but have not proven, that the sharp 1590 cm^{-1} peak in the 632 nm Raman spectrum most probably comes from semiconducting tubes in the same bundle.

In electrical transport measurements, gas exposure affects most significantly the carrier level and conductance of semiconducting nanotubes. However, in Raman measurement, this nanotube−adsorbates interaction is expected to affect mostly the Raman scattering from metallic nanotubes, because only metallic tubes have isoenergetic electronic states at the vibrational energy ~1590 cm^{-1}. The excitation of the 1590 cm^{-1} phonon by isoenergetic fast electrons was evidenced in a recent high field electrical transport measurement on metallic SWNTs.[24] In our experiment, the large Raman line shape change on doping and degassing was observed with 632 nm excitation, which probes metallic nanotubes. We did not see the similar large change with 457 nm excitation, which mainly excites semiconducting nanotubes. Note that an oxidative upshift in the tangential mode frequency for semiconducting tubes has been reported for strong oxidation with adsorbed Br_2.[25] After we exposed a degassed bundle to Br_2 vapor for a few minutes, the broadened 1540 cm^{-1} line disappeared with low power 632 nm excitation in air. Upon laser heating, the line returned as described before. This is further evidence for reversible oxidation by adsorbates.

This model of nanotube−adsorbate interaction is relevant to the resistivity difference between acid-treated and vacuum annealed SWNT sample found by Smalley group.[14] In their study, acid-treated sample showed high conductivity, while after vacuum annealing it exhibited low conductivity. In HNO_3-treated SWNT sample, we expect that charge transfer due to SWNT-doping molecule interaction oxidatively dopes nanotubes and makes ensemble sample more conductive. Once vacuum annealed, the sample is degassed and undoped, and shows higher resistivity.

B. Power-Dependent Raman Scattering. With degassed sample, we measured the Raman spectra of SWNT bundles at

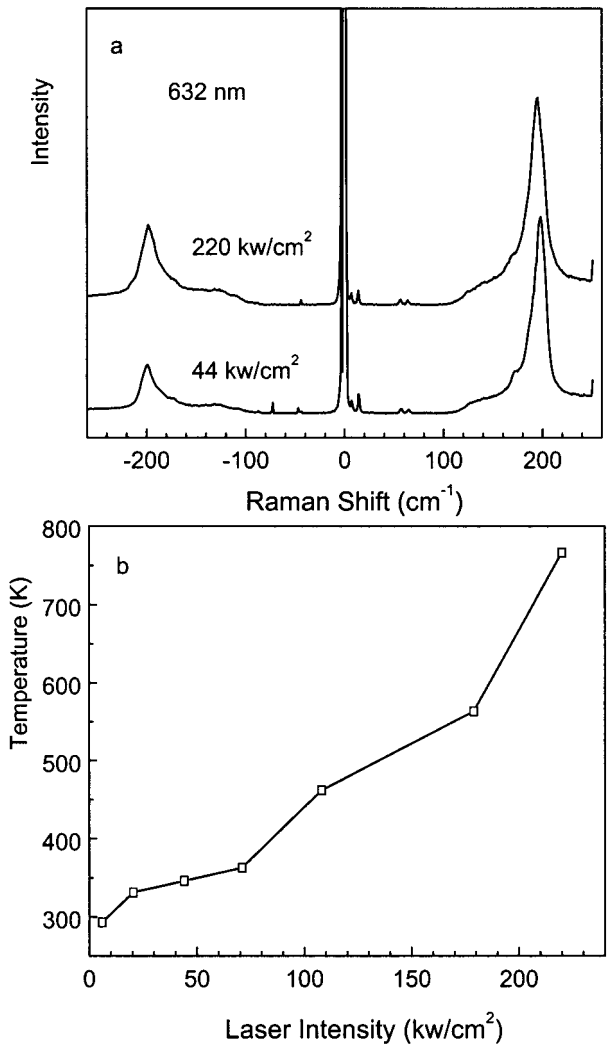

Figure 3. (a) Radial breathing mode Stokes (shown as positive Raman shift) and anti-Stokes (shown as negative Raman shift) Raman spectra of one degassed SWNT bundle at 44 kw/cm^2 (bottom) and 220 kw/cm^2 (top) excitation intensity. Their relative intensities follow a linear relation to excitation intensity (see Figure 4). (b) Sample temperature at different excitation intensities as determined on the basis of breathing mode anti-Stokes-to-Stokes Raman intensity ratio.

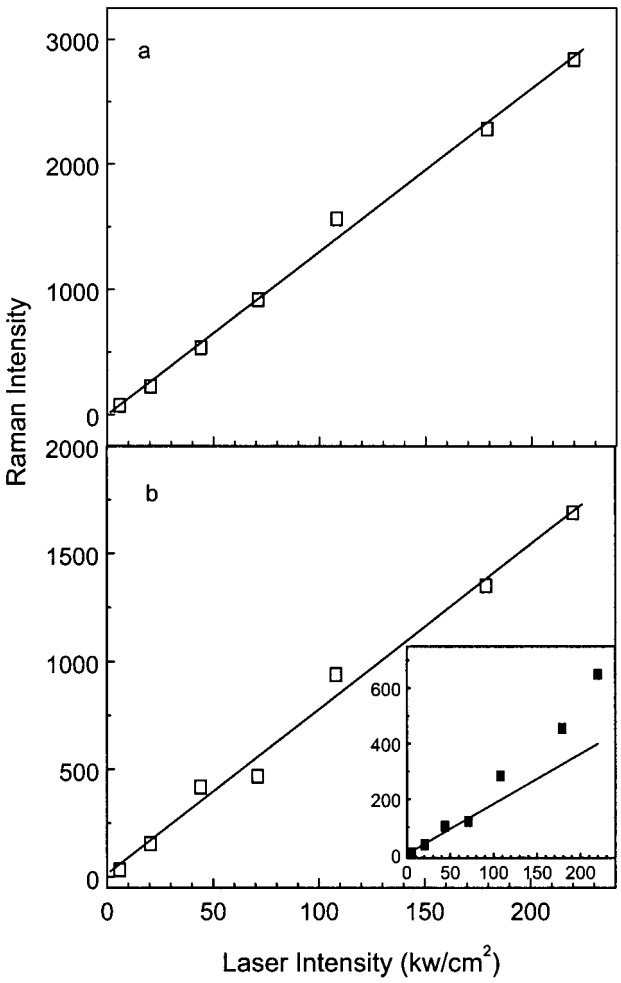

Figure 4. Power dependence of Stokes Raman scattering intensity from a single degassed SWNT bundle for (a) metallic peak at 1540 cm^{-1} and (b) radial breathing mode. Inset to (b) shows the power dependence of breathing mode anti-Stokes Raman intensity for the same rope.

different 632 nm excitation intensity. Figure 3a shows two typical Raman spectra of the breathing mode for a same bundle at excitation intensity 220 and 44 kw/cm^2, respectively. The tangential mode Raman spectra are similar to those shown in Figure 2. With increasing power, the Raman peaks are downshifted due to temperature effect. Unlike degassing, this change is reversible.

In ensemble experiments SWNT sample temperatures were reliably predicted on the basis of the ratio of the radial breathing mode (RBM) anti-Stokes-to-Stokes Raman intensity.[26] This result implies that the Stokes and anti-Stokes cross sections have the same temperature dependence. Thus, we used RBM ratio to determine the sample temperature, assuming that the temperature at lowest power level is ~300 K. This eliminates the need to calibrate the absolute response to these two Raman peaks in CCD efficiency, notch filter transmittance, and other optical components. The calculated bundle temperature at different power levels is plotted in Figure 3b. The data suggest a linear relation except for a temperature jump at the highest power level. It should be pointed out that it is difficult to get a precise relation because of the thermal drift of the bundle in the laser focusing spot. At the highest excitation power 220 kw/cm^2, our sample temperature is around 750 K. The sample temperature can also be obtained on the basis of the frequency shift of the sharp ~1590 cm^{-1} mode in semiconducting tubes.[26] The frequency shift of the 1590 cm^{-1} mode in our measurement is about 10 cm^{-1} from lowest power to highest power, which corresponds to temperature change of about 300 K, consistent with that predicted from Raman anti-Stokes-to-Stokes ratio for metallic tubes.

In Figure 3a, temperatures at 44 and 220 kw/cm^2 excitation intensity are 350 and 750 K, respectively. Due to the low vibrational energy of the RBM, the vibrational population changes substantially over this temperature range, (~44% and 68% of tubes are in excited RBM vibrational states at 350 and 750 K, respectively) and the Stokes and anti-Stokes Raman signals are superpositions of many vibrational transitions. However, peak shapes and widths are observed not to change. This observation suggests that RBM is quite harmonic.

The Stokes Raman intensity of both tangential 1540 and 1590 cm^{-1} modes, and the RBM, are linear functions of excitation intensity, as shown in Figure 4. For tangential modes at 750 K the ratio of $v = 1$ to $v = 0$ population is about 0.05. The linear dependence of tangential mode Stokes Raman suggests that 0 $\rightarrow$ 1 tangential mode Raman cross section is a constant over the temperature range from 300 to 750 K. For RBM, because of its weak anharmonicity, all the RBM Stokes transitions originating from different vibrational states appear superimposed. The linear dependence of RBM Stokes Raman suggests

that the average of Raman cross sections from different vibrational states does not change with temperature from 300 to 750 K. This is consistent with the previous ensemble study.[26] Anti-Stokes Raman of RBM, as expected, does change more than linearly with the excitation intensity, as shown in the inset of Figure 4b. However, if the temperature effect on the vibrational population is considered, we get a constant anti-Stokes Raman cross section over the temperature range in our experiment.

Conclusion

We have found that the Raman scattering of metallic carbon nanotubes depends sensitively on the processing conditions. Charge transfer due to the interaction of carbon nanotubes with oxidizing adsorbates is proposed to be responsible for the irreversible Raman change upon degassing the acid-treated sample. This model is qualitatively consistent with the conductance change of gas-exposed SWNTs in electrical transport measurement. Further, the Raman cross section of SWNTs is a constant in the temperature range 300 K−750 K, and the radial breathing mode is found quite harmonic. The large change in Raman scattering from metallic carbon nanotubes suggests that the metallic peak at 1540 cm^{-1} does represent the coupled electronic-phonon scattering. More investigation of Raman scattering from metallic nanotubes is under way to elucidate the exact mechanism of their unique Raman scattering properties.

Acknowledgment. The authors thank Prof. Jie Liu (Duke University) for the help in sample processing and Dr. Hongbin Fang for helpful discussions. We also thank Dr. Todd Krauss for his useful comments on an earlier version of this manuscript. This work was supported by the DOE under Contract FG02-98ER14861. We have used materials characterization facilities at Columbia supported by NSF MRSEC Grant DMR-98-09687. We thank the W. M. Keck foundation for a nanotechnology equipment grant.

References and Notes

(1) Iijima S.; Ichihashi T. *Nature* **1993**, *363*, 603.

(2) Bethune D. S.; Kiang C. H.; de Vries, M. S.; Goreman, G.; Savoy, R.; Vazquez, J.; Beyers, R. *Nature* **1993**, *363*, 605.

(3) Dresselhaus, M. S.; Dresselhaus, G.; Eklund, P. C. *Science of Fullerenes and Carbon Nanotubes*; Academic: San Diego, 1996.

(4) Saito, R.; Fujita, M.; Dresselhaus, G.; Dresselhaus, M. S. *Appl. Phys. Lett*. **1992**, *60*, 2204.

(5) Saito, R.; Dresselhaus, G.; Dresselhaus, M. S. *Physical Properties of Carbon Nanotubes*; Imperial College Press: Singapore, 1998.

(6) Rao, A. M.; Richter, E.; Bandow, S.; Chase, B.; Eklund, P. C.; Williams, K. A.; Fang, S.; Subbaswamy, K. R.; Menon, M.; Thess, A.; Smalley, R. E.; Dresselhaus, G.; Dresselhaus M. S. *Science* **1997**, *275*, 187.

(7) Rao, A. M.; Bandow, S.; Richter, E.; Eklund, P. C. *Thin Solid Films* **1998**, *331*, 141.

(8) Pimenta, M. A.; Marucci, A.; Brown, S. D. M.; Matthews, M. J.; Rao, A. M.; Eklund, P. C.; Smalley, R. E.; Dresselhaus, G.; Dresselhaus M. S. *J. Mater. Res*. **1998**, *57*, 4145.

(9) Saito, R.; Takeya, T.; Kimura, T.; Dresselhaus, G.; Dresselhaus M. S. *Phys. Rev. B* **1998**, *57*, 4145.

(10) Pimenta, M. A.; Marucci, A.; Empedocles, S. A.; Bawendi, M. G.; Hanlon, E. B.; Rao, A. M.; Eklund, P. C.; Smalley, R. E.; Dresselhaus, G.; Dresselhaus M. S. *Phys. Rev. B* **1998**, *58*, R16016.

(11) Kataura, H.; Kumazawa, Y.; Maniwa, Y.; Umezu, U.; Suzuki, S.; Ohtsuka, Y.; Achiba, Y. *Synth. Met.* **1999**, *103*, 2555.

(12) Duesberg, G. S.; Blau, W. J.; Byrne, H. J.; Muster, J.; Burghard, M.; Roth, S. *Chem. Phys. Lett*. **1999**, *310*, 8.

(13) Kneipp, K.; Kneipp, H.; Corio, P.; Brown, S. D. M.; Shafer, K.; Motz, J.; Perelman, L. T.; Hanlon, E. B.; Marucci, A.; Dresselhaus, G.; Dresselhaus M. S. *Phys. Rev. Lett.* **2000**, *84*, 3470.

(14) Kong, J.; Franklin, N. R.; Zhou, C.; Chapline, M. G.; Peng, S.; Cho, K.; Dai, H. *Science* **2000**, *287*, 622.

(15) Collins, P. G.; Bradley, K.; Ishigami, M.; Zettl, A. *Science* **2000**, *287*, 1801.

(16) Rinzler, A. G.; Liu J.; Dai, H.; Nikolaev, P.; Huffman, C. B.; Rodriguez-Macias, F. J.; Boul, P. J.; Lu, A. H.; Heymann, D.; Colbert, D. T.; Lee, R. S.; Fischer, J. E.; Rao, A. M.; Eklund, P. C.; Smalley, R. E. *Appl. Phys. A* **1998**, *67*, 29.

(17) Rinzler, A. G.; Hafner, J. H.; Nikolaev, P.; Lou, L.; Kim, S. G.; Tomanek, D.; Nordlander, P.; Colbert, D. T.; Smalley, R. E. *Science* **1995**, *269*, 1550.

(18) Richter, E.; Subbaswamy, K. R. *Phys. Rev. Lett*. **1997**, *79*, 2738.

(19) Petit, P.; Mathis, C.; Journet, C.; Bernier, P. *Chem. Phys. Lett*. **1999**, *305*, 370.

(20) Kazaoui, S.; Minami, N.; Jacquemin, R.; Kataura, H.; Achiba, Y. *Phys. Rev. B* **1999**, *60*, 13339.

(21) Abstreiter, G.; Cardona, M.; Pinczuk, A. Light Scattering by Free Carrier Excitations in Semiconductors. In *Light Scattering in Solids IV*; Cardona, M., Guntherodt, G., Eds.; Springer-Verlag: Berlin, Heidelberg, 1984.

(22) Ando, T.; Nakanishi, T. *J. Phys. Soc. Jpn*. **1998**, *67*, 1704.

(23) McEuen, P.; Bockrath, M.; Cobden, D.; Yoon, Y.; Louie, S. *Phys. Rev. Lett*. **1999**, *83*, 5098.

(24) Yao, Z.; Kane, C.; Dekker, C. *Phys. Rev. Lett*. **2000**, *84*, 2941.

(25) Rao, A. M.; Eklund, P. C.; Bandow, S.; Thess, A.; Smalley, R. E. *Nature* **1997**, *388*, 257.

(26) Li, H. D.; Yue, K. T.; Lian, Z. L.; Zhan, Y.; Zhou, L. X.; Zhang, S. L.; Shi, Z. J.; Gu, Z. N.; Liu, B. B.; Yang, R. S.; Yang, H. B.; Zou, G. T.; Zhang, Y.; Iijima, S. *Appl. Phys. Lett*. **2000**, *76*, 2053.